

EFFECT OF EPITAXIAL STRAIN ON THE STRUCTURAL AND FERROELECTRIC PROPERTIES OF $\text{Bi}_2\text{FeCrO}_6$ THIN FILMS

R. NECHACHE*, C. HARNAGEA, A. RUEDIGER, F. ROSEI and A. PIGNOLET

*INRS Énergie, Matériaux et Télécommunications
 1650 boulevard Lionel-Boulet
 Varennes, Québec J3X 1S2
 pignolet@emt.inrs.ca*

Received 5 March 2010; Accepted 21 March 2010

$\text{Bi}_2\text{FeCrO}_6$ thin films were epitaxially grown by pulsed laser deposition on (100)-oriented LaAlO_3 , $(\text{LaAlO}_3)_{0.3}(\text{Sr}_2\text{LaTaO}_6)_{0.7}$ and SrTiO_3 single crystalline substrates with and without epitaxial CaRuO_3 buffered layer. The in-plane compressive strain induces monoclinic distortion of the $\text{Bi}_2\text{FeCrO}_6$ lattice cell. The strain originates from lattice mismatch between CaRuO_3 and single crystal substrates. The similar crystal structure of the substrate and the layer lead to coherent epitaxial growth of the heterostructures and avoid strain relaxation in particular for BFCO films deposited on LaAlO_3 substrates. The ferroelectric character is demonstrated for all grown BFCO films. The residual in-plane strain weakly affects the effective piezoelectric coefficient of BFCO layers.

Keywords: Pulsed laser deposition (PLD); perovskite thin films; complex oxides; epitaxy; piezoresponse (PFM); crystal structure; cation ordering; double perovskite.

An important area of research in recent years has been to understand exactly why the properties of epitaxial films differ from related bulk materials, and to learn how to use these differences to engineer desirable properties. Effects due to strain in the films are often thought of as analogous to those of high pressure experiments in bulk. The main differences are (i) the stress in the films is typically biaxial rather than hydrostatic or uniaxial, (ii) films can have much larger strains than is usually achievable in pressure cells, and (iii) films are easier to work with for many experiments and applications. Ferroelectricity in strained perovskite films has been a particularly noteworthy topic of study. Recent experiments have shown strain-induced ferroelectricity in SrTiO_3 (STO) films, and huge changes in the ferroelectric transition temperature T_C in both STO and BaTiO_3 (BTO) films under strain.^{1,2} Other notable results include large changes in the metal-insulator transition temperature of NdNiO_3 films under strain³ and reports of increasing the transition temperature of $\text{La}_{2-x}\text{SrCuO}_4$ under compressive strain.⁴⁻⁶ In this letter, we present a systematic investigation of structural and ferroelectric properties in epitaxial $\text{Bi}_2\text{FeCrO}_6$ (BFCO) films with varying degree of compressive strain by using several commercially available single crystal substrates.

X-ray diffraction (XRD) patterns collected on polycrystalline BFCO film (400 nm) deposited on amorphous SiO_2 (100 nm) on Silicon (100) by laser ablation were fitted with a rhombohedral R3 unit cell similar to that previously reported for BiFeO_3 (BFO).⁷ The rhombohedral lattice parameter of this BFCO film is found to be around 5.56 Å which corresponds to a pseudo-cubic lattice parameter of ~ 3.93 Å. Recently, Suchomel *et al.* reported the synthesis of high pressure BFCO bulk.⁸ They claimed that BFCO bulk has a hexagonal R3c unit cell and the refined lattice parameters, obtained from the high resolution synchrotron XRD data are $a = 5.5454$ Å and $c = 13.6952$ Å. These values of lattice parameter are higher than those of 5.47 Å calculated by ab initio for BFCO,⁹ but slightly smaller than the value of 5.56 Å that we found for our BFCO polycrystalline film on SiO_2 on Si, which will be the reference lattice parameter for the BFCO bulk used in our study, corresponding to a pseudo-cubic lattice parameter 3.93 Å.

The BFCO films studied were grown on different substrates: LaAlO_3 (LAO), $(\text{LaAlO}_3)_{0.3}(\text{Sr}_2\text{LaTaO}_6)_{0.7}$ (LSAT), and SrTiO_3 (STO). All substrates are (100)-oriented single crystals. The mismatch between BFCO and these substrates ranges from -3.6% for LAO to -0.77% for STO.

Pulsed laser deposition (PLD) was used to grow the films. The energy density of the KrF excimer laser was

*Corresponding author.

about 2 J/cm^2 . The BFCO films were grown at 680°C in 1.2×10^{-2} mbar (9 mTorr) of oxygen, with a thickness ranging from 10 to 150 nm. To perform ferroelectric measurements, we deposited epitaxial CaRuO_3 (CRO) on the substrates as bottom electrode. CRO has an orthorhombic crystal cell with the pseudo-cubic lattice parameters about $a' = 3.85 \text{ \AA}$ and $c' = 3.83 \text{ \AA}$. The thickness of the conductive film serving as bottom electrode ranged from about 10 to 15 nm. Typical oxygen pressure of 100 mTorr and substrate temperature of $\sim 650^\circ\text{C}$ were used during growth of CRO films.

The crystal structure of the BFCO films, as well as the quality of their epitaxy, were investigated using X-Ray Diffraction (XRD) (PANalytical X'Pert MRD 4-circle diffractometer). The pseudo-cubic Miller indices of the crystal designated by brackets with a c subscript $(hkl)_c$, are used in the present study.

Local piezoelectric measurements were carried out using piezoresponse force microscopy (PFM).¹⁰⁻¹² Here we used a DI-Enviroscope atomic force microscopy (AFM) (Veeco) equipped with a NSC36a (Micromasch) cantilever and tips coated with Co/Cr. We applied an ac voltage of 0.5 V at 26 kHz between the conductive tip and the CRO layer located beneath BFCO and we detected the BFCO film surface induced piezoelectric vibrations using a lock-in amplifier from Signal Recovery (model 7265). Local hysteresis measurements as well as poling over micron-sized areas were achieved using a DC-source (Keithley 2400) to apply bias voltages to the bottom electrode of the sample.

Figure 1 shows the XRD patterns of BFCO thin films deposited on LAO(100), LSAT(100) and STO(100) substrates. Only the $(00l)_c$ diffraction peaks of the BFCO phase were observed which shows that films had a perfect c-axis orientation. Secondary phases, if any, are below the detection limit of the instrument.

The width of symmetrical rocking curves (not shown here), typically ranging between 0.1 and 0.2° , are typical of

high quality oxide films. The degree of in-plane orientation was assessed by performing XRD ϕ -scans. The results clearly indicate the presence of a four-fold symmetry for the films, i.e. a “cube-on-cube” epitaxial growth of the BFCO films on all substrates.

XRD reciprocal space maps of the BFCO films (cf. Fig. 1(b)), superimposed on the same graph, confirm the epitaxial growth. A wavelength value $\lambda = 0.15406 \text{ nm}$ for the $\text{CuK}\alpha_1$ radiation was employed to determine the Q_x and Q_z values for BFCO and to plot the reciprocal space maps.

Figure 1(b) shows XRD reciprocal space maps around the BFCO $(103)_c$ peaks for BFCO thin films deposited on $(100)\text{LAO}(100)$, $(100)\text{LSAT}(100)$ and $(100)\text{STO}(100)$ respectively.

The horizontal and vertical axes are related to the reciprocal of the in-plane and the out-of-plane lattice spacing, respectively. Due to the parallelism of BFCO and substrate axes, the Q_x and Q_z maps allow to quickly correlate the experimental results to the interplane distances and lattice parameters of the sample. The lattice spacing perpendicular to the substrates planes (d_{out}) is determined using symmetric reflections $(002)_c$, as $d_{\text{out}} = 2\pi/Q_z$. Both the out-of-plane (d_{out}) and in-plane (d_{in}) film lattice spacing are determined using asymmetric reflections (103) and (220) ($d_{\text{out}} = 2\pi/Q_z$, $d_{\text{in}} = 2\pi/Q_x$). Therefore, the mapping of one symmetric and one or two asymmetric peaks provides redundant data on lattice parameters, which are found to be consistent within experimental error.

The small condensed reciprocal point of the BFCO in all figures suggests a high quality epitaxial growth of the BFCO film on the different substrates. Moreover, this point was located at almost the same position as $\text{STO}(103)$ and $\text{LSAT}(103)$ along the horizontal axis, suggesting that the in-plane lattice parameter of the epitaxial BFCO thin films is close to those of STO and LSAT. This reveals that the strain originating from the lattice mismatch between the film and

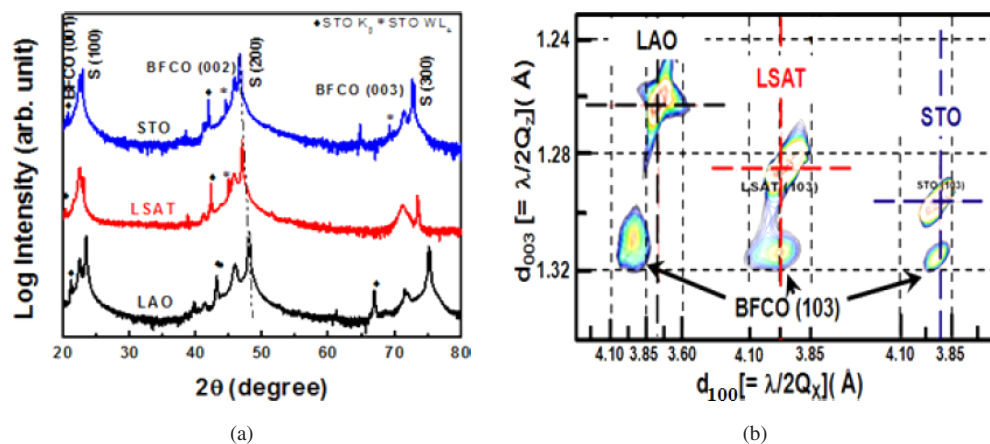


Fig. 1. (a) XRD patterns of BFCO films deposited directly on (i) LAO(100), (ii) LSAT(100), and (iii) STO(100) substrates. (b) XRD reciprocal space maps around the (103) reflection of BFCO thin films deposited on LAO(100), LSAT(100) and STO(100). Color online.

Table 1. Lattice parameters and in-plane strains of BFCO films on different substrates. The in-plane lattice parameters of substrates are LAO—3.790 Å, LSAT—3.868 Å, STO—3.905 Å. For the bulk BFCO, the pseudo-lattice parameter $a' \approx 3.93$ Å, corresponding to a cell volume of ~ 60.7 Å³.

| Thickness | BFCO | | BFCO lattice parameters (Å) | | Cell Vol. Å ³ | tetragonality (c/a)−1 | In-plane Strain |
|-----------|-------|-----------|-----------------------------|-------|-----------------------------|--------------------------|--------------------|
| | CRO | Substrate | a/b | c | | | |
| 81 nm | no | LAO | 3.921 | 3.945 | 60.6 | 0.006 | (−)0.23% |
| 78 nm | no | LSAT | 3.882 | 3.961 | 59.7 | 0.021 | (−)1.22% |
| 85 nm | no | STO | 3.902 | 3.967 | 60.4 | 0.017 | (−)0.71% |
| 80 nm | 13 nm | LAO | 3.881 | 3.966 | 59.7 | 0.022 | (−)1.27% |
| 83 nm | 13 nm | LSAT | 3.845 | 4.031 | 59.6 | 0.048 | (−)2.16% |
| 81 nm | 14 nm | STO | 3.897 | 3.965 | 60.2 | 0.017 | (−)0.84% |

(−) compressive strain.

Table 2. Lattice parameters and lattice mismatches between CRO, BFCO and the different substrates used in our study.

| Layer | Substrate | | | | |
|------------------------------------|--------------------|--------------|--------------------|-------------------|-------------------|
| | LaAlO ₃ | LSAT | SrTiO ₃ | | |
| | Lattice | Pseudo-cubic | Cubic a = 3.792 Å | Cubic a = 3.868 Å | Cubic a = 3.905 Å |
| CaRuO ₃ | Orthorhombic | | | | |
| | a = 5.36 Å | a' = 3.83 Å | (−)1.00% | (+)0.98% | (+)1.92% |
| | b = 5.53 Å | | | | |
| | c = 7.66 Å | c' = 3.85 Å | (−)1.53% | (+)0.46% | (+)1.41% |
| Bi ₂ FeCrO ₆ | Rhombohedral | | | | |
| | a = 5.56 Å | a' = 3.93 Å | (−)3.64% | (−)1.60% | (−)0.64% |

the substrate remains in the film. The in-plane and the out-of-plane values of BFCO thin film on the various substrates measured by several reciprocal space mapping are listed in Table 1. The random measurement errors in lattice parameters are less than 0.001 Å, though systematic errors may be larger. The in-plane biaxial strain is defined as $(a_{//} - a_0)/a_0$, where a_0 is the lattice parameter of bulk BFCO (~ 3.93 Å), and $a_{//}$ is the average of the lattice parameters along two in-plane axes in the strained films. The in-plane lattice parameters of BFCO were found to be different from those of the LAO substrate (3.79 Å), indicating that, in this case, the layer relaxed most of the misfit strain. The residual in-plane strain is compressive with a value of -0.23% . The out-of-plane lattice parameter rise to 3.945 Å, which is higher than that of BFCO bulk.

The bottom electrode was also deposited by PLD. We chose CaRuO₃ (CRO) because it has low resistivity (less than $300 \mu\Omega\cdot\text{cm}$) and has perovskite structure, with good lattice matching with oxide substrates and also with BFCO. The lattice parameters of CRO are listed in Table 2. Lattice mismatches between CRO, BFCO materials and the substrates used are also shown.

The thickness of CRO was limited to 10–15 nm in order to avoid strain relaxation, which would preclude the coherent growth of the heterostructure. Figure 2(a) shows XRD spectra of the heteroepitaxial BFCO/CRO thin films deposited on LAO(100) and LSAT(100) and STO(100) substrates. As seen in Fig. 2(a), only the $00l$ ($l = 1, 2, 3$) pseudocubic reflections of the films composing the BFCO/CRO heterostructure and of

the substrates are present, indicating that the oxide layers are highly (001)-oriented. No peaks suggesting secondary phases are visible in the spectra. Figure 2(b) shows XRD reciprocal space maps around the asymmetrical (204) reflection of the different substrates. The large reciprocal lattice point of the BFCO layer deposited on CRO/LAO is split in two spots for films grown on CRO/LSAT and CRO/STO. These results suggest that the BFCO unit cell is monoclinically distorted in all cases. The position of the centers of the peaks are located close to the corresponding peaks of LSAT and STO along the Q_x axis for each map, indicating that the in-plane lattice parameter of the heterostructure is very close to that of the substrate. This reveals highly strained epitaxial layers throughout the whole heterostructure, the strain originating from the lattice mismatch between the films and the substrate, as indicated in Table 2. The strain of the CRO buffered layer lead to fully coherent epitaxial growth of the heterostructure and precluding the strain relaxation especially for BFCO films deposited on LAO substrates.

Since Fe/Cr cation ordering in the BFCO double perovskite is expected only along [111] crystal direction, we performed asymmetrical $\theta-2\theta$ scans around the (111) substrate reflections. The sample was thus tilted by 54° (angle between [111] and [001] cubic directions) with respect to the surface normal. The large $\theta-2\theta$ scans (typically 18° to 70°) revealed two periodic satellite peaks at 19.5° and 61.2° , corresponding to superstructure reflections ($1/2$ $1/2$ $1/2$) and ($3/2$ $3/2$ $3/2$), in addition to main cubic reflections (111) of STO and BFCO.

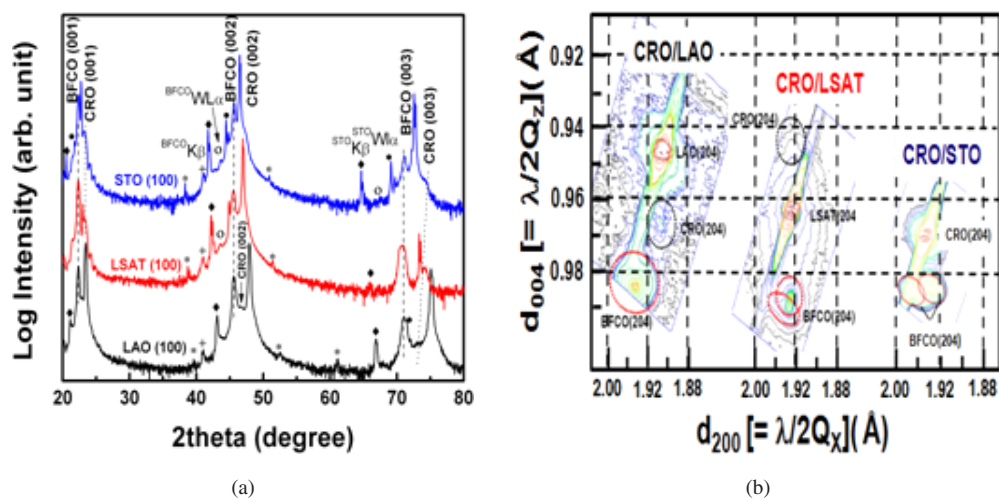


Fig. 2. (a) XRD patterns of BFCO films deposited on CRO-coated LAO(100), LSAT(100), and STO(100) substrates. (b) Corresponding XRD reciprocal space maps around the (204) reflection. Color online.

Similar satellite peaks were not observed in any other cubic directions (i.e., [110], or [100]). These superstructures reflections indicate a doubling of the crystal structure of BFCO only along the [111] direction, which is in agreement with the predicted structure. All films exhibited these superstructures, suggesting that Fe/Cr ordering was achieved in all our BFCO epitaxial thin films. To investigate the quality of the Fe/Cr cation ordering, a careful analysis of normalized intensities and shapes of superstructure peaks were carried out. Figure 3 shows the variation in the residual in-plane strain with the FWHM of the $(1/2\ 1/2\ 1/2)$ superstructure reflection and the degree of the Fe/Cr ordering. The latter is estimated from the normalized ratio of the superlattice peaks intensities to the main (111) reflection intensity of BFCO in the pseudo-cubic indexing. As can be seen in Fig. 3, the cation ordering (blue squares) is only weakly affected by strain.

Since the ordering is highly sensitive to the growth temperature,¹³ this result can be explained by the fact that the optimum temperature deposition is almost the same for all heterostructures, with low fluctuations, and the thermal absorption coefficient is almost similar for all the substrates. On the other hand, we observed a broadening of the superstructure peaks when the residual strain was reduced in the films. For double perovskites, an increase of FWHM of the superstructure reflections is usually due to the formation in the films of stacking defects, such as antiphase boundaries (APBs). In general, the strain relaxation in thin films with perovskite structure implies the nucleation of misfit dislocations and the formation of grain boundaries in thin films. These crystal defects favor the formation of APBs in the grown layers and their densities increase with strain relaxation. This explains the variation in the superstructure shape observed in our case.

The effect of strain on the local ferroelectric properties of BFCO films was investigated via PFM.

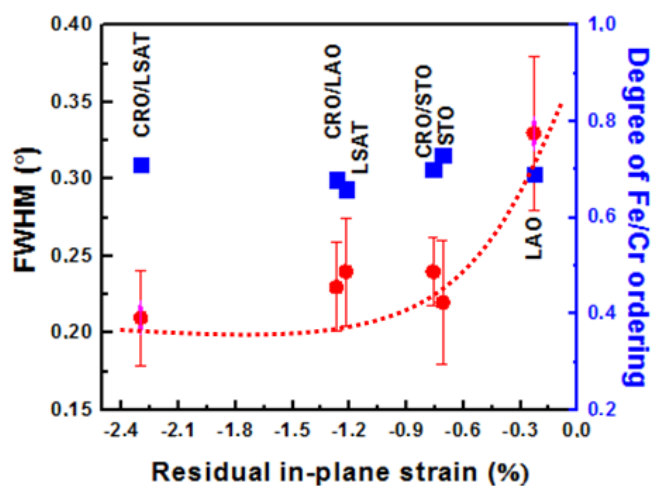


Fig. 3. Dependence of the FWHM of the superstructure peak $(1/2\ 1/2\ 1/2)$ on the residual in-plane strain — read dots, and degree of Fe/Cr ordering — blue squares, for BFCO epitaxial films grown on different substrates. Color online.

First, we poled areas of the BFCO layer “up” and “down”, by applying alternatively positive and negative voltages (8 V) between the conductive AFM tip and the CRO bottom electrode. PFM was then used to visualize the induced domain structure. Figure 4(a) shows the PFM images of the 80 nm thick-BFCO film before (left) and after writing (right). We observe a well-defined contrast in the PFM images that clearly shows the presence of up and down ferroelectric domains in all films. To further prove the ferroelectric character of our films and also to compare the ferroelectric behavior, we recorded local piezoelectric hysteresis loops, by keeping the AFM tip fixed above a desired location, in contact with the sample surface. Here we present remanent hysteresis loops, obtained as described in Ref. 14 (Fig. 4(b)). The strength of the PFM signal is comparable to that obtained from BFO films.¹⁵ The effective

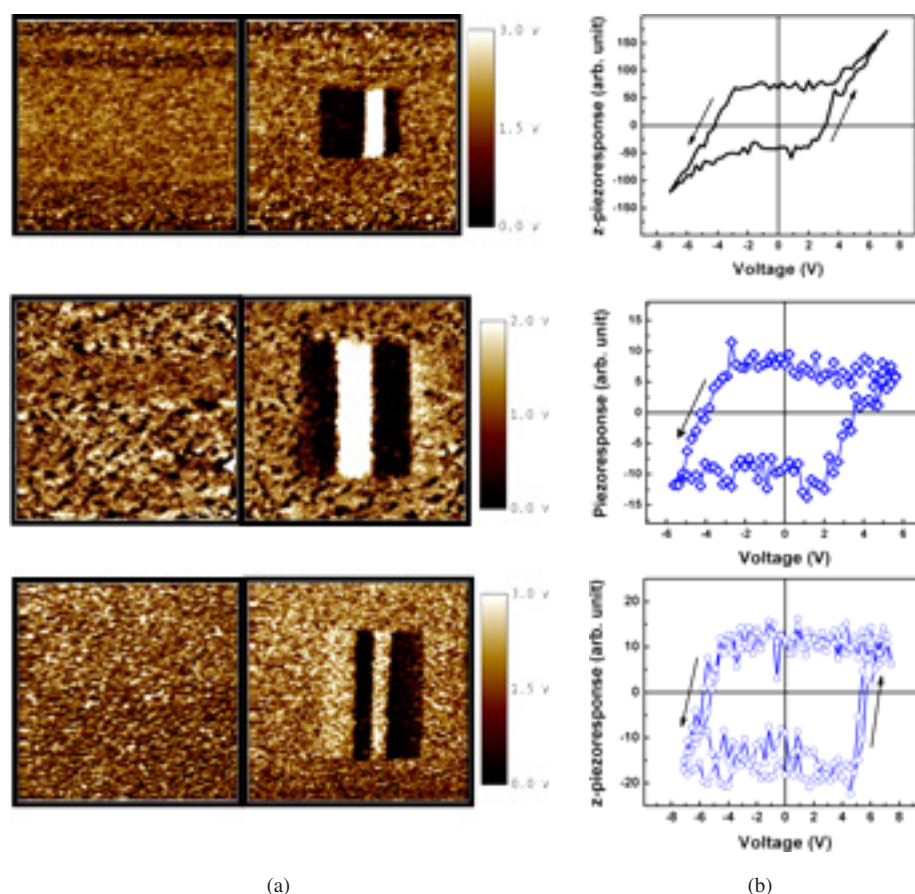


Fig. 4. Local ferroelectric characterization of a BFCO film. For BFCO thin films deposited on: from top to bottom LAO(100), LSAT(100) and STO(100). (a) PFM image before (left) and after (right) writing oppositely polarized domains using the AFM tip as a top electrode (black/white contrast represents polarization oriented upwards/downwards). Scan size of the images is $5 \times 5 \mu\text{m}^2$. (b) Local remanent piezoresponse hysteresis, for BFCO thin films deposited on: from top to down, LAO(100), LSAT(100) and STO(100) — with the same convention as in (a) — using an epitaxial 15 nm thick-CRO buffer layer as bottom electrode. Color online.

piezoelectric coefficient of the BFCO/CRO heterostructures (d_{zz}) is estimated from the PFM signal. The plot of d_{zz} coefficient vs. the residual in-plane strain (curve not shown here) revealed a weak correlation between them. Indeed, the d_{zz} coefficient is weakly affected by the modification of strain in the heterostructures, which is in agreement with results previously reported for some ferroelectric perovskites.¹⁶

In conclusion, we have heteroepitaxially grown BFCO single layers, either on CRO-buffered (100)-oriented STO, LSAT and LAO substrates or directly on (100)-oriented STO, LSAT and LAO substrates, using PLD. Due to the in-plane compressive strain, all films have a monoclinically distorted crystal structure in contrast to the bulk counterpart. When deposited directly on LAO, the BFCO epitaxial films relax, but interestingly, when deposited on a CRO buffer layer, the BFCO/CRO/LAO heterostructure is coherent throughout. This might be attributed to the tensile strain of the CRO layer epitaxially grown on LAO.

The ferroelectric character of the epitaxial BFCO layer has been demonstrated for all films grown on all substrates.

It has also been shown that the residual in-plane strain only weakly affects both the Fe/Cr cation ordering and the effective piezoelectric coefficient of BFCO layers. Since BFCO is a multiferroic material, strain might also affect the magnetic properties, and further investigations of strain effect on the magnetic properties on BFCO films are currently in progress. The possibility of controlling the growth of nanoscale BFCO structures through a nanostensils also represents an exciting perspective for the future work.^{17,18}

Acknowledgments

We acknowledge financial support from Canada Foundation for Innovation. F.R. is grateful to FQRNT and the Canada Research Chairs Program for partial salary support. F.R. and A.P. are supported by discovery grants (NSERC).

References

1. J. H. Haeni *et al.*, *Nature* **430**, 758 (2004).
2. K. J. Choi *et al.*, *Science* **306**, 1005 (2004).
3. A. Tiwari, C. Jin and J. Narayan, *Appl. Phys. Lett.* **80**, 4039 (2002).

88 R. Nechache et al.

4. H. Sato and M. Naito, *Physica C* **274**, 221 (1997).
5. W. Si, H.-C. Li and X. X. Xi, *Appl. Phys. Lett.* **74**, 2839 (1999).
6. I. Bozovic, G. Logvenov, I. Betca, B. Narimbetov and I. Sveklo, *Phys. Rev. Lett.* **89**, 107001 (2002).
7. F. Kubel and H. Schmid, *Acta Crystallogr., Sect. B: Struct. Sci. B* **46**, 698 (1990).
8. M. R. Suchomel, C. I. Thomas, M. Allix, M. J. Rosseinsky and A. M. Fogg, *Appl. Phys. Lett.* **90**, 112909 (2007).
9. P. Baettig, C. Ederer and N. Spaldin, *Phys. Rev. B* **72**, 214105 (2005).
10. C. Harnagea, A. Pignolet, M. Alexe, D. Hesse and U. Gosele, *Appl. Phys. A* **70**, 261 (2000).
11. K. Franke, J. Besold, W. Haessler and C. Seegebarth, *Surf. Sci. Lett.* **302**, L283 (1994).
12. A. Gruverman, O. Auciello and H. Tokumoto, *Annu. Rev. Mater. Sci.* **28**, 101 (1998).
13. R. Nechache, C. Harnagea, L.-P. Carignan, O. Gautreau, L. Pintilie, M. P. Singh, D. Ménard, P. Fournier, M. Alexe and A. Pignolet, *J. Appl. Phys.* **105**, 061621 (2009).
14. C. Harnagea, C. V. Cojocaru, R. Nechache, O. Gautreau, F. Rosei and A. Pignolet, *Int. J. Nanotechnol.* **5**, 930 (2008).
15. R. Nechache, P. Gupta, C. Harnagea and A. Pignolet, *Appl. Phys. Lett.* **91**, 222908 (2007).
16. Y. H. Chu, T. Zhao, M. P. Crus, Q. Zhan, P. L. Yang, L. W. Martin, M. Huijben, C. H. Yang, F. Zavaliche, H. Zheng and R. Ramesh, *Appl. Phys. Lett.* **90**, 252906 (2001).
17. C. V. Cojocaru, C. Harnagea, F. Rosei, A. Pignolet, M. A. F. van den Boogaart and J. Brugger, *Appl. Phys. Lett.* **86**, 183107 (2005).
18. C. V. Cojocaru, C. Harnagea, A. Pignolet and F. Rosei, *IEEE Trans. Nanotechnol.* **5**, 470 (2006).